This article has been accepted for publication in a future issue of this journal, but has not been fully edited. Content may change prior to final publication. Citation information: DOI 10.1109/JSTARS.2021.3120013, IEEE Journal of Selected Topics in Applied Earth Observations and Remote Sensing



# Impacts of Satellite Revisit Frequency on Spring Phenology Monitoring of Deciduous Broad-leaved Forests based on Vegetation Index Time Series

Jiaqi Tian, Xiaolin Zhu, Luoma Wan, Melissa Collin

***Abstract*—Satellites have different revisit frequencies (i.e., temporal resolutions), ranging from daily to monthly. The satellite revisit frequencies suitable for accurately monitoring the phenology of deciduous broad-leaved forests (DBF) are not well-known. To fill this knowledge gap, this study used MODIS Daily Nadir BRDF-Adjusted images to simulate EVI time series with a wide range of temporal resolutions from daily to 52 days, to investigate the impacts of satellite revisit frequency on monitoring spatial and temporal patterns of spring phenology, i.e., the start of season (SOS), of DBF in North America. Then, these EVI time series were used to extract SOS by two common phenology extraction methods (i.e., relative threshold and curvature methods). Our results reveal that (1) low temporal resolutions cannot accurately reconstruct real vegetation growth profile, which generally causes a false early SOS detection, (2) the impact of temporal resolutions is nonlinear. The accuracy of SOS detection from data with relatively high frequencies (e.g., 7 days) is only slightly lower than that from daily time series but the accuracy decreases largely with low frequencies, and (3) validation with ground observations from PhenoCam Network stations and an experiment using three real satellite datasets (i.e., MODIS, Landsat 8, and Sentinel-2) confirm the findings from our simulation study. This study suggests that satellites with medium temporal resolutions, such as Sentinel-2 and Landsat 8, could extract reliable phenology metrics in non-cloudy regions.**

***Index Terms*—Start of season, SOS, EVI time series, satellite revisit frequency, temporal resolution**

## I. Introduction

The start of season (SOS), also named spring phenology, one of the most critical recurring growth phases of vegetation dynamics, has been documented as an effective indicator of regional environmental condition change (e.g., precipitation, temperature, and photoperiod) [1]–[3] and large-scale climate change (e.g., global warming) [4], [5]. Also, it is highly related to plant productivity, crop yield, carbon and water cycling [6]–[9]. Accurately detecting the phenological shifts is crucial for exploring how vegetation phenology responds to these environmental variables. Owing to large spatial coverage and multi-year consecutive observations, satellite data has been broadly adopted to measure SOS by using various satellite-derived vegetation index (VI) time series, such as normalized difference vegetation index (NDVI), enhanced vegetation index (EVI), enhanced vegetation index 2 (EVI2), and normalized difference phenology index (NDPI), to record the vegetation growth trajectory [10]–[13].

In recent years, the number of earth observation satellites with medium/high spatial resolutions is increasing. Compared with the traditional daily data (e.g., MODIS) for vegetation phenology detection, these medium/high spatial resolution data generally have lower revisit frequencies, such as ENVISAT (35 days), SPOT (26 days), Landsat (16 days), Sentinel-2 A/B (5 days) and Gaofen-1 (4 days). Thus, the construction of the VI time series is greatly limited by satellite revisit frequency. Meanwhile, due to the latitude zones and weather effects (e.g., cloud covers) [14]–[16], temporal resolutions of available images are generally much coarser than the satellite revisit frequency. For example, a previous study [15] found that for Landsat 7 ETM+, 37% of the global land scenes collected less than 6 images each year, which is far less than the regular 16-day temporal resolution. For the daily satellite images, such as MODIS and AVHRR, the maximum value composite (MVC) method has been conventionally used to reduce the impact of clouds in satellite images, but two studies found that the MVC composition window can affect the phenology accuracy [16], [17]. MVC cannot be used to solve the cloud cover issues in the satellite images with lower frequencies. Based on this, we hypothesize that different satellite revisit frequencies may create uncertainties in spatial and temporal phenological detection results extracted by satellite-derived VI time series.

Manuscript received ###. This study was supported in part by the National Science Foundation of China under project 42022060, in part by the Hong Kong Polytechnic University, under Project ZVN6, and in part by the Research Institute for Sustainable Urban Development, the Hong Kong Polytechnic University, under Project BBWD (*Corresponding author: Xiaolin Zhu*).

Jiaqi Tian and Luoma Wan are with the Department of Land Surveying and Geo-Informatics, The Hong Kong Polytechnic University, 999077, Hong Kong, China (e-mail: jackie.tian@connect.polyu.hk; roma@link.cuhk.edu.hk).

Xiaolin Zhu is with the Department of Land Surveying and Geo-Informatics and the Research Institute for Sustainable Urban Development, The Hong Kong Polytechnic University, 999077, Hong Kong, China (e-mail: xiaolin.zhu@polyu.edu.hk).

Melissa Collin is with the Department of Environmental Science & Management, Humboldt State University, Arcata, California, United States (e-mail: melissa.collin@humboldt.edu).

It is widely accepted that lower revisit frequencies can reduce the accuracy of phenology detection, but the explicit relationship between satellite revisit frequency and phenology accuracy is unknown. To fill this research gap, the objectives of this study are: (1) to investigate how EVI temporal resolutions affect SOS detection of deciduous vegetation in terms of spatial and temporal dimensions, (2) to validate SOS results derived from EVI time series of different temporal resolutions by ground observations, and (3) to provide suggestion on the selection of satellite data with suitable temporal resolutions for phenology detection. To achieve above objectives, this study will use simulated EVI time series with a wide range of temporal resolutions, ranging from daily to 52 days, to determine SOS of deciduous broad-leaved forests (DBF) using two phenology extraction methods (i.e., relative threshold and curvature methods). The daily EVI time series were calculated from the MODIS Daily Nadir BRDF-Adjusted Reflectance products, and the EVI time series of other temporal resolutions, ranging from 4-52 days, were resampled from the daily EVI time series.

## II. Study Area

The study area is a region mosaicked by four MODIS tiles (h11v04, h11v05, h12v04, and h12v05), as shown in Figure 1. It covers the region of Great Lakes in North America, including the large DBF areas. The DBF has strong seasonality and observable phenological patterns, which is one of the main target vegetation types to explore and understand the mechanisms of how vegetation phenology responds to climate change over the northern hemisphere [17], [18].

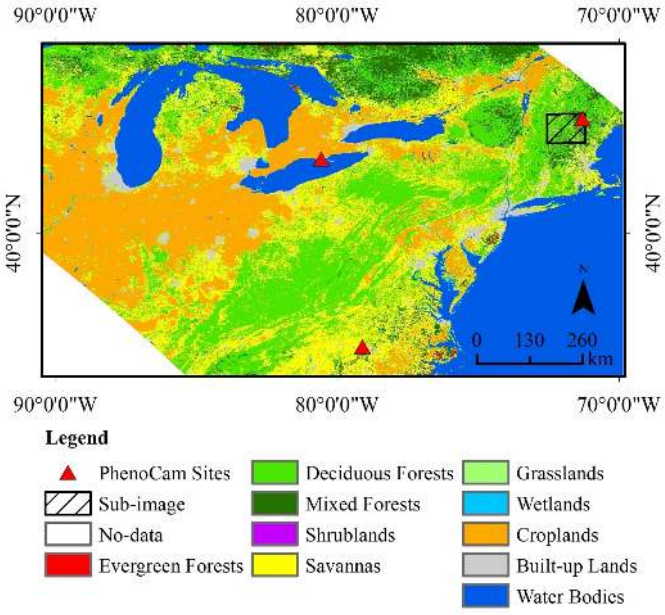


Fig. 1. The location of the study area and spatial pattern of land cover types retrieved from MODIS Land Cover Type product (MCD12Q1) in 2018. The PhenoCam sites and sub-image were used to validate the results.

## III. Data Used

Three main types of datasets, MODIS Daily Nadir BRDF-Adjusted Reflectance (NBAR) products, MODIS Land Cover Type MCD12Q1 products, and the PhenoCam Network digital photographs were employed in this study. The details of each dataset are introduced in the following sub-sections.

### A. MODIS Daily Nadir BRDF-Adjusted Reflectance

MODIS Daily NBAR products at 500 m resolution provide the cloud-free MODIS bands 1-7 (Red, Green, Blue, NIR, and three SWIR bands) and three broad bands (0.3-0.7μm, 0.7-5.0μm, and 0.3-5.0μm) [19]. The NBAR directional reflectance has good stability and consistency because the effects of satellite sensor viewing angles are removed [20]. Moreover, the NBAR values are being directly adopted as the original input to the RandomForest classifiers used in the production of the global MODIS Land Cover Product MCD12Q1. NBAR data has been utilizing in cases where composited surface reflectance products have traditionally been applied. [19]. The data can be found and downloaded via: https://lpdaac.usgs.gov/data/.

### B. MODIS Land Cover Type MCD12Q1 products

MODIS Land Cover Type MCD12Q1 provides yearly global land cover types with a spatial resolution of 1 km since 2001, derived from six different classification schemes [21]. We used the MCD12Q1 International Geosphere-Biosphere Programme (IGBP) aggregated into 17 main categories including 11 natural vegetation classes, three developed and mosaic lands classes, and three non-vegetation lands classes. The classification accuracy of IGBP is well performed and qualitatively realistic according to the validation by high-resolution imagery at global and regional scales [22]. Its classification scheme has also been widely applied to studies of satellite phenology monitoring [23], [24]. We resampled the MODIS MCD12Q1 map into a 500 m grid to match MODIS NBAR products using the nearest neighbor method. The data can be accessed from the website: https://lpdaac.usgs.gov/data/.

### C. PhenoCam Network digital photographs

The PhenoCam Network is a cooperative continental-scale phenological observatory that uses imagery from networked digital cameras to track vegetation phenology in a diverse range of ecosystems across North America and all over the world (https://phenocam.sr.unh.edu/webcam/). The digital images of the PhenoCam Network were frequently used to monitor vegetation dynamics because of the high collecting frequency and reduced external effects from clouds and the atmosphere [11], [25]. In this study, we selected three PhenoCam Network stations of type I sites (i.e., data being the highest quality) to assess and validate phenological results extracted from satellite-based EVI time series. Details of the three PhenoCam stations are summarized in Table I.

TABLE I.

DETAILS OF THREE PHENOCAM STATIONS USED

| No. | Sites | Period | Lat./Lon. | Elevation |
|---|---|---|---|---|
| 1 | bartlettir | 2009-2016 | 44.07, -71.29 | 268 m |
| 2 | turkeypointdbf | 2013-2017 | 42.64, -80.56 | 211 m |
| 3 | dukehw | 2014-2019 | 35.97, -79.10 | 400 m |

* The locations of three sites are Bartlett Experimental Forest, Bartlett, New Hampshire (bartlettir), Mature Deciduous Site, Turkey Point Carbon Cycle Research Project, Ontario, Canada (turkeypointdbf), and Hardwood Stand, Duke Forest, North Carolina (dukehw), respectively.

## IV. METHODS

### A. Generating daily EVI time series

Diverse satellite-derived VI time series (e.g., NDVI, EVI, EVI2 and NDPI) were developed and employed to extract the vegetation phenology metrics [10]–[13]. By comparison, the EVI has several advantages: (1) the accuracy of phenological metrics determined by MODIS EVI has been broadly validated by ground observations [26], [27], and (2) EVI can minimize the effects of signals from the background of vegetation canopy and maintain the sensitivity of vegetation dynamics [28]. Consequently, we calculated the daily EVI time series using three bands (Blue, Red, and NIR) of MODIS NBAR products, as:

$$\mathrm{EVI} = \mathrm{G} \times \frac{(NIR - Red)}{(NIR + C_1 \times Red - C_2 \times Blue + L)} \quad (1)$$

where Blue, Red and NIR refer to the NBAR values in the MODIS Blue, Red, and NIR bands, respectively. $L = 1$ is the canopy background adjustment, the $C_1 = 6$ and $C_2 = 7.5$ are aerosol resistance coefficients, and the $\mathrm{G} = 2.5$ is a gain factor. Snow may cover vegetation canopy causing EVI values decrease [29]. Thus, after the generation of cloud-free daily EVI time series, we further screened snow contaminated pixels flagged by the MODIS snow cover product (MOD10A1). To remove snow effects, we used the median of clear EVI values in winter (November-March) as background value to replace snow contaminated values for each pixel of DBF [30]. Last, the missing or fill values of EVI time series were interpolated using linear interpolation of the two nearest clear EVI values [31].

### B. Generating EVI time series of different temporal resolutions

EVI time series of different temporal resolutions from daily to 52 days are required to be conducted in this study. Some satellites, e.g., ENVISAT (35 days), SPOT (26 days), Landsat (16 days), Sentinel-2 A/B (5 days) and Gaofen-1 (4 days), can provide data of different temporal resolutions, but are still limited. Also, the differences between these satellite sensors in spatial resolutions, sensor configurations, and atmospheric conditions at the time of acquiring images will lead to uncertainties when exploring the effects of temporal resolution on phenology detection. As a result, EVI time series of different temporal resolutions, including 4 days, 7 days, 10 days, 13 days, 16 days, 19 days, 22 days, 25 days, 28 days, 31 days, 34 days, 37 days, 40 days, 43 days, 46 days, 49 days and 52 days, were resampled from daily EVI time series, and the EVI value of the first day is preserved. Last, EVI time series with temporal resolutions coarser than daily were filled to daily by cubic spline for the subsequent SOS detection [32]–[35].

### C. Extracting SOS

We adopted two conventional phenology extraction methods (i.e., relative threshold and curvature methods) to define pixel-based SOS of DBF derived from each EVI temporal resolution. The relative threshold method identifies SOS with a predefined threshold (e.g., 10%, 15%) of vegetation growth amplitude, while the curvature method defines the inflexion point of the vegetation growth profile as SOS [36]. To extract SOS, three steps are involved. The 1st step is to smooth EVI time series by removing outliers, noises, and undetected cloud effects using the Savizky-Golay (SG) filter. The SG filter accurately maintained primary shapes and features of VI time series (e.g., maximum, minimum, and amplitude) [37], [38], and the smoothed EVI profiles using SG filter has been validated using ground truth observations [39]. The 2nd step is to fit the curve (the red lines shown in Figure 2) using a four-parameter logistic function (Equation (2)). This depiction can accurately reflect the trajectory of vegetation growth and dynamics [27]. The 3rd step is to determine SOS using the relative threshold method and curvature method, respectively (Figure 2). We used a threshold of 10% to define the SOS for the relative threshold method in this study. Then, the rate of change of curvature (RCC) was calculated using Equation (3), and the date was defined as SOS for the curvature method when RCC came to its first maximum value [27].

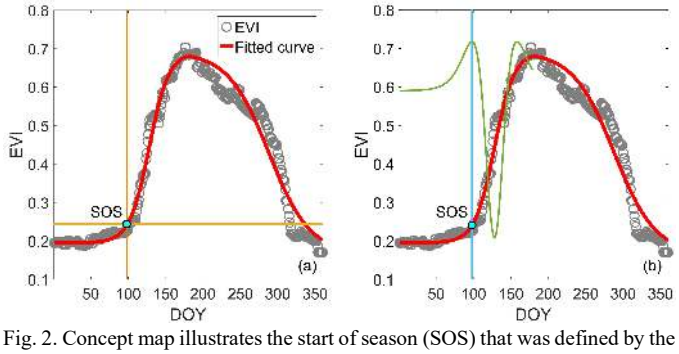


Fig. 2. Concept map illustrates the start of season (SOS) that was defined by the relative threshold method (a) and curvature method (b) at a DBF pixel (coordinate: 34.96, -84.58). DOY: day of year.

$$y(t) = \frac{c}{1 + e^{a+bt}} + d \quad (2)$$

where $t$ is the time in the day of year (DOY), $y(t)$ is the fitted EVI value at date $t$, $a$ and $b$ represent the fitting parameters, $c + d$ is the maximum EVI value, and $d$ is the initial background EVI value.

$$RCC = b^3 cz\left\{\frac{3z(1-z)(1+z)^3[2(1+z)^3+b^2c^2z]}{[(1+z)^4+(bcz)^2]^{2.5}} - \frac{(1+z)^2(1+2z-5z^2)}{[(1+z)^4+(bcz)^2]^{1.5}}\right\} \quad (3)$$

where $z = e^{a+bt}$.

### *D. Analyzing the relationship between SOS and temporal resolutions and quantifying interannual variations of SOS*

This study adopted the linear and quadratic polynomial regression models, respectively, to analyze the relationship between SOS and temporal resolutions. Furthermore, we calculated the long-term trends derived from SOS values to quantify the interannual variations of SOS using a linear regression model, as Equation (4):

$$y = ax + b \quad (4)$$

where $y$ is the SOS, $x$ is the year order from 1 to $n$, $a$ is the slope (i.e., long-term trend), and $b$ is the intercept term, determined by the least square method [40]. This trend is a simple but effective proxy to describe the interannual variations of SOS [17], [30], [40]. The positive or negative trend means the delayed or advanced SOS with years, respectively.

### *E. Assessing the accuracy of SOS extracted by EVI time series of different temporal resolutions*

To assess the accuracy of SOS results extracted by EVI time series of different temporal resolutions, we used the digital photographs from PhenoCam Network stations (i.e., ground observations) that were widely used to monitor vegetation phenology and dynamics [41]. Compared with satellite remotely sensed images, the digital repeat photographs are free of cloud and atmosphere and have extremely high temporal resolutions (typically, half an hour). In this study, we used three PhenoCam stations of type I (i.e., data being the highest quality) of DBF, named bartlettir, turkeypointdbf, and dukehw (as Table I). The views and regions of interest (ROI) of PhenoCam sites were shown in Figure 3. In processing of PhenoCam data, the green chromatic coordinate (GCC) that reflects relative brightness was computed first by Equation (5):

$$GCC = \frac{G}{R+G+B} \quad (5)$$

Parameters $R$, $G$, and $B$, which refer to Red, Green, and Blue digital numbers (DNs), were extracted from the ROI of PhenoCam imagery, indicating the relative brightness in these wavelengths (Figure 3). Similarly, the GCC SOS were extracted by the relative threshold and curvature methods, described in section IV-C. Last, we calculated the absolute difference (D) of SOS of each year and mean absolute difference (MAD) of multi-year SOS between EVI SOS extracted by different temporal resolutions and GCC SOS at each PhenoCam site.

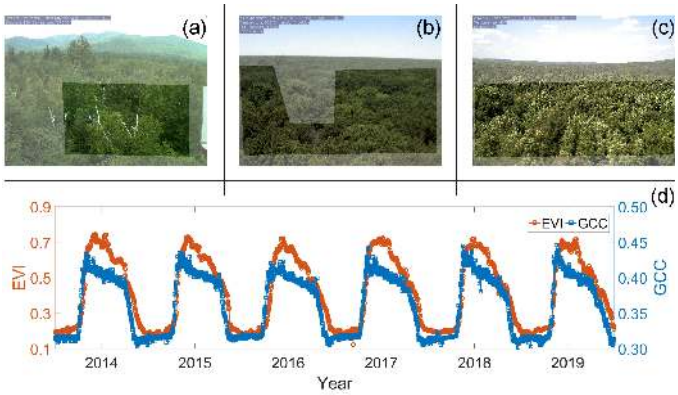


Fig. 3. Views and regions of interest (ROI) of three PhenoCam Network stations: bartlettir (a), turkeypointdbf (b), and dukehw (c), and raw EVI and GCC time series during 2014 to 2019 at PhenoCam site: dukehw (d).

## V. RESULTS

### *A. Spatial patterns of SOS extracted by EVI time series of different temporal resolutions*

Figure 4 shows the spatial distributions of SOS derived from the EVI time series of several representative temporal resolutions by relative threshold and curvature methods, respectively, and the color bar is unified. It is reasonable to assume that SOS derived from daily cloud-free EVI time series (hereafter named as "daily-derived SOS") is most accurate because daily cloud-free EVI time series can sufficiently reflect the vegetation growth trajectory. We accordingly identified the daily-derived SOS as a reference value (i.e., benchmark). First, there is a clear latitudinal gradient pattern from daily-derived SOS using two methods in our study area, i.e., earlier SOS in southern regions and later SOS in northern regions (Figure 4). Also, the spatial patterns of SOS from EVI time series with medium temporal resolutions (e.g., 7 days and 16 days) have high consistency with that of daily-derived SOS. However, this consistency decreases with coarser temporal resolutions, particularly when temporal resolutions are coarser than 16 days. For example, it is hard to recognize a similar gradient pattern to that of the daily-derived SOS from the SOS extracted from the 37-day EVI time series. With regards to the differences in extraction methods, the highly consistent spatial patterns of SOS extracted by both methods (Figure 4) suggest the robustness between the two methods.

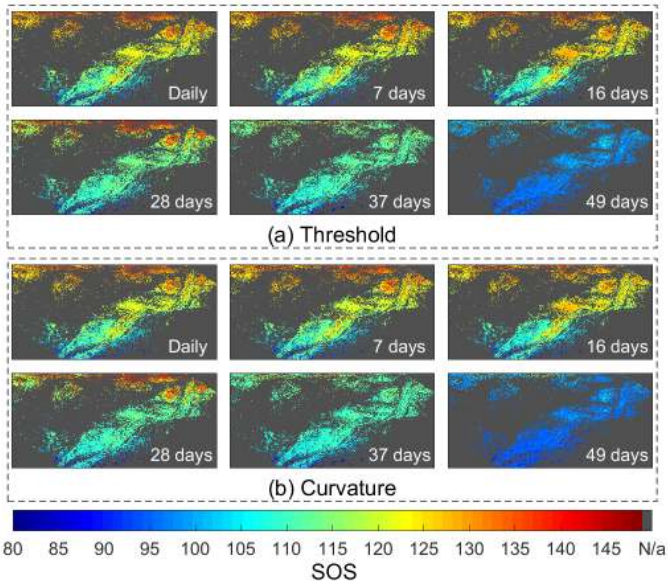


Fig. 4. Spatial distributions of SOS extracted from EVI time series of several representative temporal resolutions by relative threshold method (a) and curvature method (b).

We further quantified the SOS results extracted by EVI time series of each temporal resolutions from daily to 52 days over the entire study area, as shown in Figure 5. Two regression models, namely the linear regression model and the quadratic polynomial model, were used to explore the relationship between SOS and temporal resolutions. We found that the quadratic polynomial model is better than the linear regression model to describe the relationship with $R^2$ of 0.919 over 0.809 for the relative threshold method and 0.918 over 0.808 for the curvature method, respectively. More specifically, the results of SOS (i.e., earlier SOS) generally decrease along with the drop in temporal resolutions (Figure 5). However, compared with daily-derived SOS (i.e., reference lines in Figure 5), the results of SOS start to become rather stable when the temporal resolution is up to 16 days.

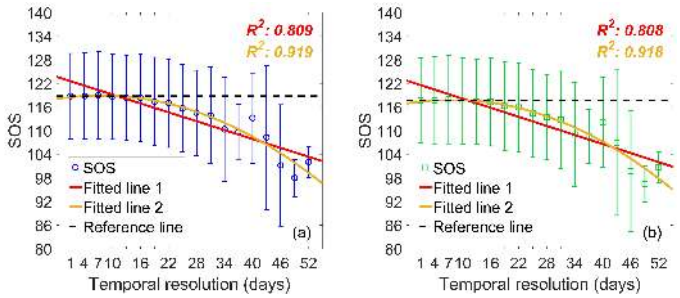


Fig. 5. Average SOS extracted by EVI time series of different temporal resolutions over the entire study area using relative threshold method (a) and curvature method (b), and red and yellow lines determined by least square method indicate the fitted lines by linear regression model and quadratic polynomial regression model, respectively. Reference lines refer to the average of daily-derived SOS.

### *B. Interannual variations of SOS extracted by EVI time series with different temporal resolutions*

The interannual variations of SOS at three PhenoCam sites (i.e., bartlettir, turkeypointdbf, and dukehw) were retrieved from the EVI time series with different temporal resolutions (Figure 6). Compared with interannual variations of daily-derived SOS, it shows the dramatically inconsistent fluctuations when using coarser temporal resolutions (as bars shown in Figure 6), suggesting that uncertainties and errors may be introduced because of coarser temporal resolutions. Moreover, we computed the long-term trends to quantify the interannual variations of SOS, shown as red and blue lines with square markers in Figure 6. It uncovers that the long-term trends of SOS may be misestimated when using coarse temporal resolutions, particularly for coarser than 16 days. As an example of turkeypointdbf station, the long-term trends derived from the daily to 16-day temporal resolutions have similar negative values (i.e., earlier SOS with years), but became positive values (i.e., later SOS with years) or values with greater bias when using temporal resolutions coarser than 16 days (Figure 6). In addition, it shows that the interannual variations of SOS extracted by EVI time series of different temporal resolutions show high consistency no matter which extraction method was used.

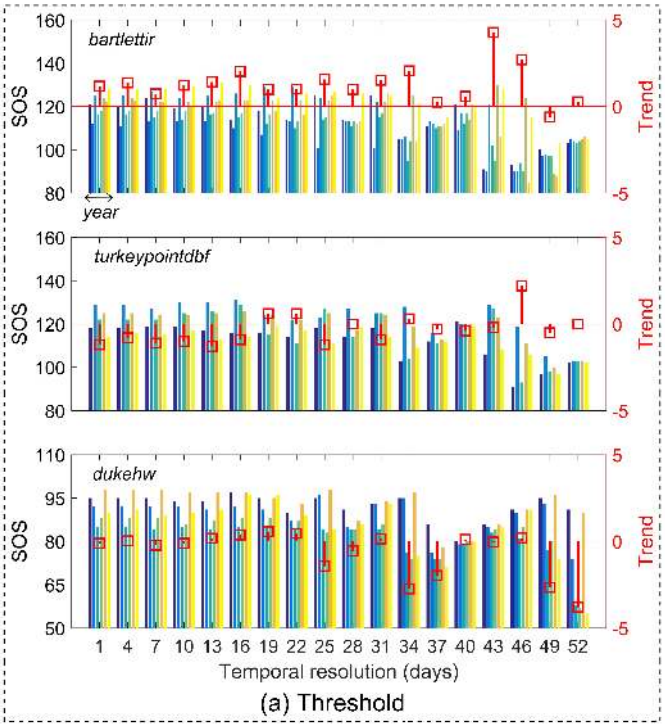

This article has been accepted for publication in a future issue of this journal, but has not been fully edited. Content may change prior to final publication. Citation information: DOI 10.1109/JSTARS.2021.3120013, IEEE Journal of Selected Topics in Applied Earth Observations and Remote Sensing



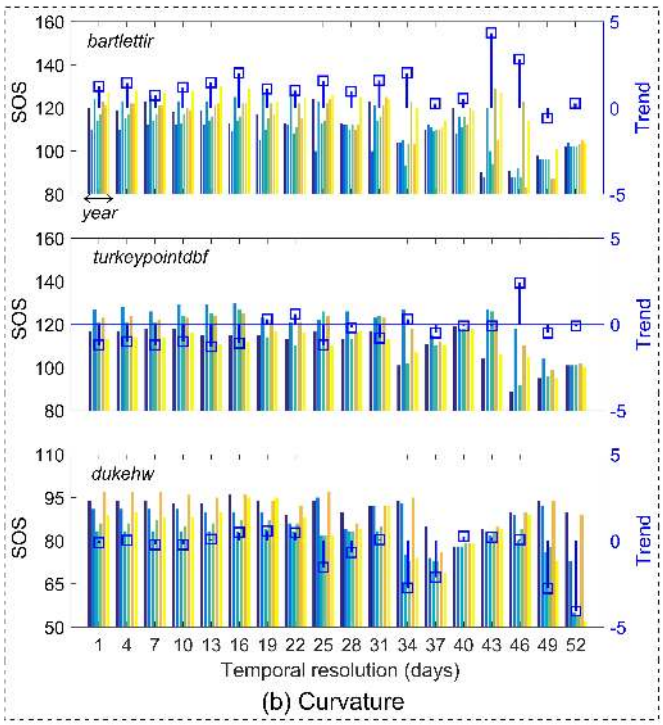


Fig. 6. Interannual variations of SOS at three PhenoCam Network stations extracted by EVI time series of different temporal resolutions using relative threshold method (a) and curvature method (b). The red and blue lines with square markers refer to the long-term trends (days/year) of SOS.

### C. *Validation at PhenoCam Network stations*

Considering the limited accuracy of SOS estimated by satellite-based EVI time series, we further used GCC SOS derived from the PhenoCam Network photographs to validate the results of EVI SOS derived from different temporal resolutions, as shown in Table II. It indicates that the accuracy (i.e., MADs) of SOS generally shows a decreasing trend as temporal resolutions being coarser, but high consistency of accuracy of SOS (MADs: around 5 days) is maintained for finer temporal resolutions from daily to 16 days.

TABLE II.
ABSOLUTE DIFFERENCES BETWEEN EVI SOS EXTRACTED BY EVI TIME SERIES OF DIFFERENT TEMPORAL RESOLUTIONS AND GCC SOS AT THREE PHENOCAM NETWORK SITES USING THE RELATIVE THRESHOLD METHOD (UNIT: DAYS)

| Site | Year | Temporal resolution (unit: days) | | | | | | | | | | | | | | | | | |
|---|---|---|---|---|---|---|---|---|---|---|---|---|---|---|---|---|---|---|---|
| | | 1 | 4 | 7 | 10 | 13 | 16 | 19 | 22 | 25 | 28 | 31 | 34 | 37 | 40 | 43 | 46 | 49 | 52 |
| 1 | 2009 | 2 | 1 | 5 | 0 | 1 | 5 | 1 | 5 | 6 | 5 | 6 | 14 | 8 | 2 | 28 | 26 | 19 | 16 |
| | 2010 | 1 | 2 | 0 | 0 | 0 | 3 | 6 | 0 | 12 | 0 | 12 | 8 | 0 | 4 | 23 | 23 | 16 | 8 |
| | 2011 | 1 | 1 | 3 | 0 | 1 | 2 | 5 | 5 | 0 | 11 | 2 | 18 | 12 | 7 | 3 | 34 | 26 | 20 |
| | 2012 | 0 | 0 | 1 | 2 | 0 | 1 | 4 | 6 | 2 | 5 | 1 | 21 | 6 | 4 | 14 | 22 | 19 | 13 |
| | 2013 | 1 | 1 | 1 | 1 | 2 | 2 | 3 | 6 | 4 | 6 | 2 | 15 | 8 | 2 | 24 | 29 | 22 | 15 |
| | 2014 | 4 | 4 | 6 | 6 | 6 | 5 | 5 | 5 | 5 | 16 | 6 | 3 | 17 | 14 | 2 | 4 | 39 | 23 |
| | 2015 | 0 | 1 | 0 | 2 | 1 | 1 | 4 | 6 | 3 | 9 | 4 | 18 | 10 | 1 | 16 | 37 | 34 | 16 |
| | 2016 | 2 | 2 | 2 | 1 | 1 | 0 | 6 | 4 | 3 | 4 | 5 | 9 | 15 | 10 | 2 | 15 | 27 | 25 |
| 2 | 2013 | 5 | 5 | 4 | 4 | 6 | 7 | 7 | 9 | 5 | 9 | 5 | 20 | 11 | 2 | 17 | 32 | 26 | 21 |
| | 2014 | 6 | 6 | 8 | 5 | 5 | 4 | 11 | 13 | 12 | 8 | 10 | 7 | 19 | 15 | 6 | 16 | 30 | 32 |
| | 2015 | 3 | 3 | 3 | 0 | 1 | 4 | 10 | 14 | 2 | 11 | 0 | 21 | 14 | 5 | 2 | 32 | 27 | 22 |
| | 2016 | 8 | 8 | 9 | 9 | 8 | 7 | 9 | 11 | 8 | 16 | 9 | 14 | 20 | 13 | 10 | 22 | 33 | 30 |
| | 2017 | 17 | 15 | 16 | 14 | 18 | 17 | 12 | 14 | 20 | 12 | 17 | 22 | 19 | 12 | 23 | 25 | 34 | 29 |
| 3 | 2014 | 5 | 5 | 5 | 4 | 4 | 7 | 5 | 0 | 5 | 1 | 3 | 5 | 4 | 10 | 4 | 1 | 5 | 1 |
| | 2015 | 3 | 3 | 3 | 3 | 2 | 3 | 2 | 2 | 7 | 4 | 4 | 6 | 13 | 10 | 4 | 1 | 4 | 15 |
| | 2016 | 14 | 14 | 13 | 14 | 13 | 14 | 14 | 13 | 13 | 13 | 13 | 5 | 3 | 8 | 12 | 10 | 6 | 13 |
| | 2017 | 6 | 6 | 6 | 4 | 5 | 6 | 6 | 5 | 1 | 2 | 4 | 8 | 8 | 2 | 2 | 3 | 2 | 25 |
| | 2018 | 8 | 8 | 8 | 7 | 7 | 7 | 5 | 3 | 8 | 3 | 4 | 7 | 12 | 10 | 4 | 1 | 6 | 0 |
| | 2019 | 3 | 4 | 2 | 3 | 4 | 9 | 9 | 2 | 3 | 1 | 6 | 12 | 16 | 7 | 2 | 4 | 13 | 32 |
| MAD | | 4.7 | 4.7 | 5.0 | 4.2 | 4.5 | 5.5 | 6.5 | 6.5 | 6.3 | 7.2 | 5.9 | 12.3 | 11.3 | 7.3 | 10.4 | 17.7 | 20.4 | 18.7 |

* Sites 1, 2 and 3 are bartlettir, turkeypointdbf and dukehw PhenoCam stations, respectively. MAD: mean absolute difference.

## VI. DISCUSSION

### A. *Possible reasons causing SOS differences due to temporal resolutions*

According to our results (Figure 5), coarse temporal resolutions can generally underestimate the results of SOS, meaning the coarser the temporal resolutions, the earlier the SOS. To explore the underlying reasons causing this underestimation of SOS, we first calculated the average daily EVI time series of DBF over the entire study area so that the effects from the noises and undetected contamination pixels can be removed. Several EVI time series of representative temporal resolutions including 4 days, 13 days, 25 days, 40 days, and 52 days were obtained from the daily EVI time series (described in section IV-B). Afterwards, the SOS were extracted from these EVI time series using relative threshold and curvature methods, described in section IV-C. Compared with reference lines (i.e., daily-derived SOS), the results of SOS when using coarse

temporal resolutions were generally underestimated (i.e., earlier SOS) and became more severe with coarser resolution (Figure 7). Also, it shows that the EVI time series of coarse temporal resolutions cannot recover actual vegetation growth trajectory (see the differences between green and red lines in Figure 7). According to previous studies [27], [42], the fitted parameter "*a*" can control the translation of EVI time series, parameter "*b*" is related to the increasing rate of EVI, and parameter "*c*" (i.e., amplitude of EVI time series) reflects the vegetation growth speed. We, thus, summarized the parameters of fitted lines derived from the logistic function, as Equation (2), into Table III. It reveals that both parameters "*a*" and "*b*" show a monotonic trend from daily to 52 days, suggesting a systematic shifting of the VI time series with satellite revisit frequencies, which leads to the bias in SOS detection. In addition, the parameter "*c*" depending on the EVI amplitude shows a constantly decreasing trend as temporal resolutions being coarser, which may result in the misestimation of the vegetation growth speed. Overall, we assumed that the potential reason causing SOS differences due to different temporal resolutions is that the EVI time series of coarse temporal resolutions cannot describe vegetation growth profile accurately. This is mainly because longer data intervals (i.e., coarser temporal resolutions) may skip or ignore the key phases of vegetation growth that are crucial for SOS extraction, thus results in inaccurate estimation of SOS.

TABLE III.
STATISTICS OF SOS AND PARAMETERS OF FITTED LINES OF SEVERAL REPRESENTATIVE TEMPORAL RESOLUTIONS

| Temporal resolution | SOS[1] | SOS[2] | RMSE | *a* | *b* | *c* |
|---|---|---|---|---|---|---|
| daily | 116 | 115 | - | 16.389 | -0.123 | 0.470 |
| 4 days | 115 | 114 | 0.001 | 16.096 | -0.121 | 0.470 |
| 13 days | 114 | 113 | 0.006 | 15.070 | -0.113 | 0.469 |
| 25 days | 112 | 110 | 0.014 | 13.346 | -0.100 | 0.466 |
| 40 days | 110 | 109 | 0.014 | 11.932 | -0.088 | 0.464 |
| 52 days | 105 | 104 | 0.039 | 11.745 | -0.091 | 0.455 |

* SOS[1] and SOS[2] refer to the results of SOS (unit: DOY) extracted by the relative threshold method and curvature method, respectively. The fitted parameters *a* and *b* are derived from the logistic function as Equation (2). The parameter *c* is the amplitude of the EVI time series. The RMSE means the fitted accuracy between the fitted EVI time series of different temporal resolutions and fitted lines derived from daily EVI time series.

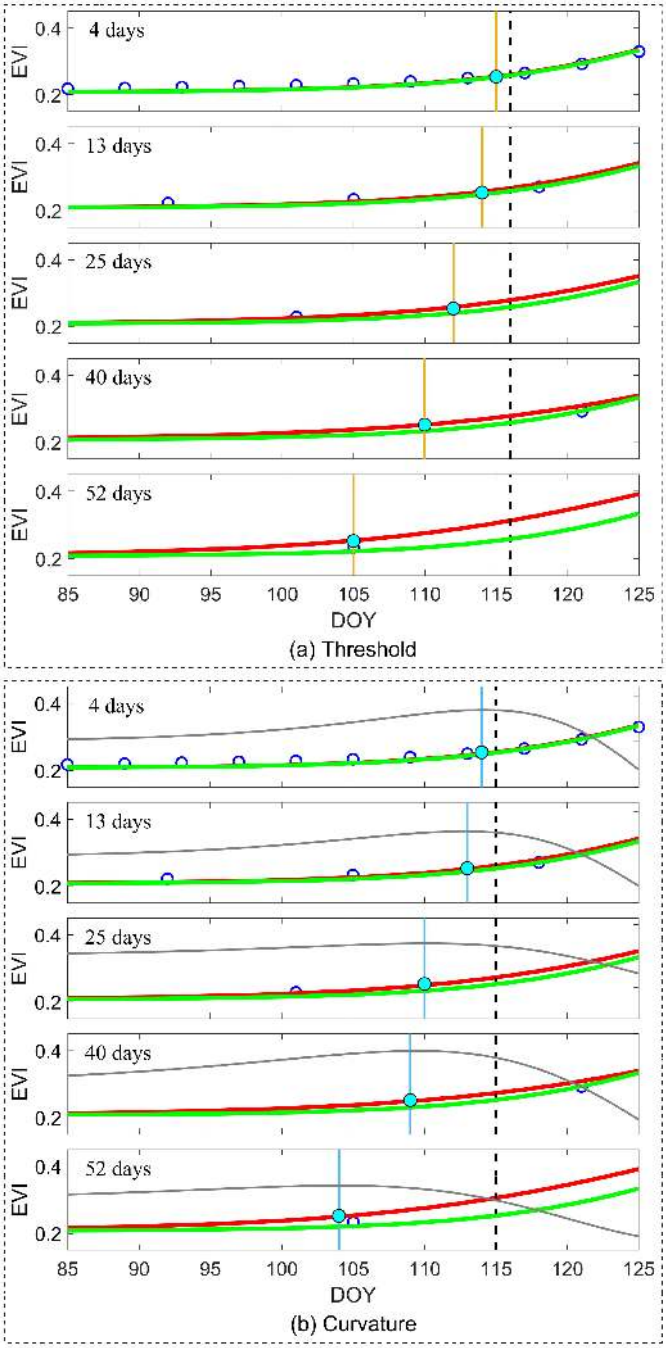


Fig. 7. The principle of SOS extracted by EVI time series of several representative temporal resolutions using relative threshold method (a) and curvature (b) method. The black dotted lines are daily-derived SOS, and the grey lines indicate the RCC values calculated by Equation (3). The blue hollow points are EVI data points. The red lines are fitted by EVI time series of different temporal resolutions while the green fitted lines are derived from daily EVI time series. DOY: day of year.

### *B. Comparison of SOS results derived from actual satellite data with different revisit frequencies*

We further compared and analyzed the SOS results of a small sub-image (marked by a box in Figure 1) extracted by actual satellite data (i.e., MODIS, Landsat 8, and Sentinel-2) with different revisit frequencies, as shown in Figure 8. The Landsat 8 OLI/TIRS level 2 surface reflectance data (path: 13 and row: 30) and Sentinel-2 L1C top-of-atmosphere (TOA) radiance data

(tile: T18TYP) with cloud cover less than 20% in 2018 were downloaded via: https://earthexplorer.usgs.gov/. Also, we used the official software Sen2Cor to produce Sentinel-2 L2A surface reflectance data to eliminate atmospheric effects [33]. To match with MODIS results, we resampled the surface reflectance data (i.e., Blue, Red and NIR bands) of Landsat 8 and Sentinel-2 into the same spatial resolution with MODIS NBAR products by the pixel aggregation method. Afterwards, these surface reflectance data were used to calculate EVI, described in section IV-A, and the SOS values were derived from EVI time series by two phenology extraction methods, described in section IV-C. Figure 8 shows that the SOS results derived from satellite data with different temporal resolutions have inconsistent spatial patterns. More specifically, longer temporal resolutions (Landsat 8 and Sentinel-2) generally cause earlier SOS extraction results than that of daily satellite data (MODIS), which is similar to the findings of our simulation experiment (Figure 5).

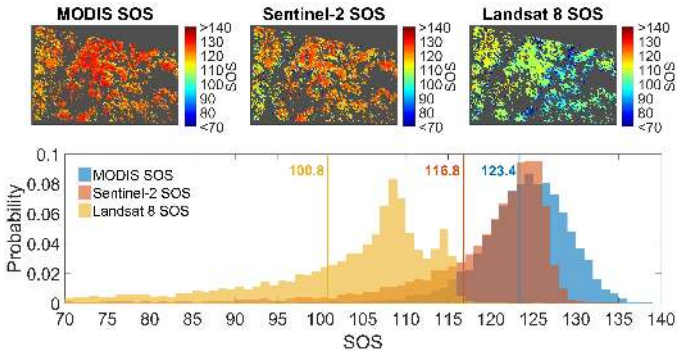


Fig. 8. Spatial patterns of SOS derived from the EVI time series of MODIS, Sentinel-2 and Landsat 8 using the relative threshold method. The histogram summarizes the SOS values extracted by MODIS, Sentinel-2 and Landsat 8 EVI time series, and the yellow, orange and blue solid lines indicate the mean of SOS results.

### C. *Implications and limitations*

The temporal resolution of satellite-derived VI time series is greatly limited by satellite revisit frequencies. Meanwhile, satellite images are severely affected by latitude zones and cloud covers, resulting in the big spatial heterogeneity of data availability [14]–[16]. As a result, the available images used to generate VI time series are far less than regular satellite revisit frequencies in some actual situations. Additionally, it is not well-known what satellite revisit frequencies are more suitable for monitoring the phenology of DBF spatially and temporally. Our results show that the coarse temporal resolutions generally can obtain biased SOS, particularly for temporal resolutions coarser than 16 days (Figure 5 and Figure 6). This means that the existing studies on SOS detection of DBF with coarser temporal resolutions may contain uncertainties and errors. Based on our findings, temporal resolutions finer than or equal to 16 days are reliable to be used to extract highly accurate SOS results of DBF in non-cloudy regions, thereby suggesting that satellites with medium temporal resolutions, such as Landsat 8 and Sentinel-2, can extract reliable SOS of DBF. In addition, we found that the EVI time series with coarser temporal resolutions (> 16 days) cannot recover the actual vegetation growth trajectory and extract accurate SOS. In some cases, there are not enough available cloud-free images to construct a dense VI time series, we suggest using cutting-edge techniques to reconstruct high-quality VI time series, for example, gap-filling [43] and data fusion algorithms [44]–[46] rather than directly using temporally sparse images.

This study comes with several limitations. First, we only focused on the DBF with strong seasonality. For other vegetation types, e.g., evergreen forests, grasslands, shrubs, and crops, our findings need further verification. Secondly, our study area is not seriously affected by the cloud issue [16], so the cloud-cleared MODIS NBAR data and time series smoothing step in the phenology detection can largely remove the effect of cloudy observations in the daily time series. However, the uncertainty in daily MODIS data may affect the results. Also, for other areas with high cloud frequency, the results may contain uncertainty caused by cloud effects and further studies are needed. Thirdly, we only explored the impacts of satellite revisit frequency on spring phenology. Other vegetation phenological metrics, like autumn phenology, could have been considered since they are also crucial to understand the mechanism of interaction between vegetation and climate change [18]. Based on this, a comprehensive study to explore the impacts of satellite revisit frequency on more vegetation types and phenological metrics is necessary for future research.

## VII. Conclusion

The temporal resolution of the EVI time series is important to monitor the spatial and temporal patterns of spring phenology of DBF accurately. This study aimed to investigate the impact of temporal resolution of EVI time series on DBF phenology monitoring. The results showed that EVI time series of temporal resolutions finer than or equal to 16 days are appropriate to detect SOS of DBF spatially and temporally in non-cloudy regions and can achieve highly consistent accuracy (i.e., MADs) with ground observations in North America. This result can support further work on SOS detection of DBF in terms of temporal resolution selection and affirm that satellite images with medium temporal resolutions, such as Landsat 8 and Sentinel-2, have the potential for monitoring vegetation phenology in non-cloudy areas.

## ACKNOWLEDGMENT

The authors would like to thank Miss. Yi Nam Xu for proofreading the manuscript.

## References

[1] J. Bennie, T. W. Davies, D. Cruse, and K. J. Gaston, "Ecological effects of artificial light at night on wild plants," *Journal of Ecology*, vol. 104, no. 3, pp. 611–620, 2016.

[2] N. Cong *et al.*, "Spring vegetation green-up date in China inferred from SPOT NDVI data: A multiple model analysis," *Agricultural and Forest Meteorology*, vol. 165, pp. 104–113, 2012.

[3] M. Shen, S. Piao, N. Cong, G. Zhang, and I. A. Jassens, "Precipitation impacts on vegetation spring phenology on the Tibetan Plateau," *Global Change Biology*, vol. 21, no. 10, pp. 3647–3656, 2015.

[4] C. Parmesan, "Influences of species, latitudes and methodologies on

estimates of phenological response to global warming," *Global Change Biology*, vol. 13, no. 9, pp. 1860–1872, 2007.

[5] T. Root, J. Price, K. Hall, and S. Schneider, "Fingerprints of global warming on wild animals and plants," *Nature*, vol. 421, no. 6918, pp. 57–60, 2003.

[6] M. R. Anwar *et al.*, "Climate change impacts on phenology and yields of five broadacre crops at four climatologically distinct locations in Australia," *Agricultural Systems*, vol. 132, pp. 133–144, 2015.

[7] D. Baldocchi, E. Falge, and L. Gu, "FLUXNET: A new tool to study the temporal and spatial variability of ecosystem-scale carbon dioxide, water vapor, and energy flux densities," *Bulletin of the American Meteorological Society*, no. February, 2001.

[8] T. F. Keenan *et al.*, "Net carbon uptake has increased through warming-induced changes in temperate forest phenology," *Nature Climate Change*, vol. 4, no. 7, pp. 598–604, 2014.

[9] A. D. Richardson *et al.*, "Influence of spring and autumn phenological transitions on forest ecosystem productivity," *Philosophical Transactions of the Royal Society B: Biological Sciences*, vol. 365, no. 1555, pp. 3227–3246, 2010.

[10] A. Vrieling *et al.*, "Vegetation phenology from Sentinel-2 and field cameras for a Dutch barrier island," *Remote Sensing of Environment*, vol. 215, no. November 2017, pp. 517–529, 2019.

[11] C. Wang *et al.*, "A snow-free vegetation index for improved monitoring of vegetation spring green-up date in deciduous ecosystems," *Remote Sensing of Environment*, vol. 196, pp. 1–12, 2017.

[12] X. Zhang *et al.*, "Exploration of scaling effects on coarse resolution land surface phenology," *Remote Sensing of Environment*, vol. 190, pp. 318–330, 2017.

[13] D. Zhou, S. Zhao, L. Zhang, and S. Liu, "Remotely sensed assessment of urbanization effects on vegetation phenology in China's 32 major cities," *Remote Sensing of Environment*, vol. 176, pp. 272–281, 2016.

[14] A. M. Wilson and W. Jetz, "Remotely Sensed High-Resolution Global Cloud Dynamics for Predicting Ecosystem and Biodiversity Distributions," *PLOS Biology*, pp. 1–20, 2016.

[15] J. Ju and D. P. Roy, "The availability of cloud-free Landsat ETM+ data over the conterminous United States and globally," *Remote Sensing of Environment*, vol. 112, pp. 1196–1211, 2008.

[16] J. Tian *et al.*, "Improving the accuracy of spring phenology detection by optimally smoothing satellite vegetation index time series based on local cloud frequency," *ISPRS Journal of Photogrammetry and Remote Sensing*, vol. 180, no. May, pp. 29–44, 2021.

[17] C. Wang and K. Zhu, "Misestimation of Growing Season Length Due to Inaccurate Construction of Satellite Vegetation Index Time Series," *IEEE Geoscience and Remote Sensing Letters*, vol. 16, no. 8, pp. 1185–1189, 2019.

[18] M. Shen, N. Jiang, D. Peng, Y. Rao, and Y. Huang, "Can changes in autumn phenology facilitate earlier green-up date of northern vegetation ?," *Agricultural and Forest Meteorology*, vol. 291, no. June 2019, p. 108077, 2020.

[19] C. Schaaf *et al.*, "MODIS MCD43 Product User Guide V005."

[20] C. B. Schaaf *et al.*, "First operational BRDF , albedo nadir reflectance products from MODIS," *Remote Sensing of Environment*, vol. 83, pp. 135–148, 2002.

[21] D. Sulla-menashe and M. A. Friedl, "User Guide to Collection 6 MODIS Land Cover ( MCD12Q1 and MCD12C1 ) Product," no. Figure 1, pp. 1–18, 2018.

[22] M. A. Friedl, D. K. Mciver, J. C. F. Hodges, X. Y. Zhang, D. Muchoney, and A. H. Strahler, "Global land cover mapping from MODIS : algorithms and early results," *Remote Sensing of Environment*, vol. 83, pp. 287–302, 2002.

[23] X. Li, Y. Zhou, G. R. Asrar, J. Mao, X. Li, and W. Li, "Response of vegetation phenology to urbanization in the conterminous United States," *Global Change Biology*, vol. 23, no. 7, pp. 2818–2830, 2016.

[24] Q. Ren, C. He, Q. Huang, and Y. Zhou, "Urbanization Impacts on Vegetation Phenology in China," *Remote Sensing*, vol. 10, p. 1095, 2018.

[25] E. K. Melaas, J. A. Wang, D. L. Miller, and M. A. Friedl, "Interactions between urban vegetation and surface urban heat islands : a case study in the Boston metropolitan region Interactions between urban vegetation and surface urban heat islands : a case study in the Boston metropolitan region," *Environmental Research Letters*, vol. 11, 2016.

[26] A. Huete, K. Didan, T. Miura, E. P. Rodriguez, X. Gao, and L. G. Ferreira, "Overview of the radiometric and biophysical performance of the MODIS vegetation indices," *Remote Sensing of Environment*, vol. 83, no. 195–213, 2002.

[27] X. Zhang *et al.*, "Monitoring vegetation phenology using MODIS," *Remote sensing of environment*, vol. 84, no. 3, pp. 471–475, 2003.

[28] M. Dallimer, Z. Tang, P. R. Bibby, P. Brindley, K. J. Gaston, and Z. G. Davies, "Temporal changes in greenspace in a highly urbanized region," *Biology letters*, no. February, pp. 763–766, 2011.

[29] X. Zhang, "Reconstruction of a complete global time series of daily vegetation index trajectory from long-term AVHRR data," *Remote Sensing of Environment*, vol. 156, pp. 457–472, 2015.

[30] M. Shen, G. Zhang, N. Cong, S. Wang, W. Kong, and S. Piao, "Increasing altitudinal gradient of spring vegetation phenology during the last decade on the Qinghai-Tibetan Plateau," *Agricultural and Forest Meteorology*, vol. 189–190, no. April, pp. 71–80, 2014.

[31] X. Zhang, M. A. Friedl, and C. B. Schaaf, "Global vegetation phenology from Moderate Resolution Imaging Spectroradiometer (MODIS): Evaluation of global patterns and comparison with in situ measurements," *Journal of Geophysical Research: Biogeosciences*, vol. 111, no. 4, pp. 1–14, 2006.

[32] D. K. Bolton, J. M. Gray, E. K. Melaas, M. Moon, L. Eklundh, and M. A. Friedl, "Continental-scale land surface phenology from harmonized Landsat 8 and Sentinel-2 imagery," *Remote Sensing of Environment*, vol. 240, no. January, p. 111685, 2020.

[33] J. Tian *et al.*, "Investigating the urban-induced microclimate effects on winter wheat spring phenology using Sentinel-2 time series," *Agricultural and Forest Meteorology*, vol. 294, no. August, p. 108153, 2020.

[34] Y. T. Solano-Correa, F. Bovolo, L. Bruzzone, and D. Fernandez-Prieto, "A Method for the Analysis of Small Crop Fields in Sentinel-2 Dense Time Series," *IEEE Transactions on Geoscience and Remote Sensing*, vol. 58, no. 3, pp. 1–15, 2019.

[35] M. A. White *et al.*, "Intercomparison, interpretation, and assessment of spring phenology in North America estimated from remote sensing for 1982-2006," *Global Change Biology*, vol. 15, no. 10, pp. 2335–2359, 2009.

[36] R. Shang, R. Liu, M. Xu, Y. Liu, L. Zuo, and Q. Ge, "The relationship between threshold-based and in fl exion-based approaches for extraction of land surface phenology," *Remote Sensing of Environment*, vol. 199, pp. 167–170, 2017.

[37] J. Chen, P. Jönsson, M. Tamura, Z. Gu, B. Matsushita, and L. Eklundh, "A simple method for reconstructing a high-quality NDVI time-series data set based on the Savitzky-Golay filter," *Remote Sensing of Environment*, vol. 91, no. 3–4, pp. 332–344, 2004.

[38] Z. Cai, P. Jönsson, H. Jin, and L. Eklundh, "Performance of smoothing methods for reconstructing NDVI time-series and estimating vegetation phenology from MODIS data," *Remote Sensing*, vol. 9, no. 12, pp. 20–22, 2017.

[39] L. Chu, Q. sheng Liu, C. Huang, and G. huan Liu, "Monitoring of winter wheat distribution and phenological phases based on MODIS time-series: A case study in the Yellow River Delta, China," *Journal of Integrative Agriculture*, vol. 15, no. 10, pp. 2403–2416, 2016.

[40] J. Chen *et al.*, "A Simple Method for Detecting Phenological Change From Time Series of Vegetation Index," *IEEE Transactions on Geoscience and Remote Sensing*, vol. 54, no. 6, pp. 3436–3449, Jun. 2016.

[41] A. D. Richardson *et al.*, "Tracking vegetation phenology across diverse North American biomes using PhenoCam imagery," *SCIENTIFIC DATA*, pp. 1–24, 2018.

[42] L. Liu, R. Cao, M. Shen, J. Chen, J. Wang, and X. Zhang, "How Does Scale Effect Influence Spring Vegetation Phenology Estimated from Satellite-Derived Vegetation Indexes ?," pp. 1–20, 2019.

[43] X. Zhu, F. Gao, D. Liu, and J. Chen, "A modified neighborhood similar pixel interpolator approach for removing thick clouds in landsat images," *IEEE Geoscience and Remote Sensing Letters*, vol. 9, no. 3, pp. 521–525, 2012.

[44] Y. Qiu, J. Zhou, J. Chen, and X. Chen, "Spatiotemporal fusion method to simultaneously generate full-length normalized difference vegetation index time series ( SSFIT )," *International Journal of Applied Earth Observations and Geoinformation*, vol. 100, p.

102333, 2021.

[45] X. Zhu, J. Chen, F. Gao, X. Chen, and J. G. Masek, "An enhanced spatial and temporal adaptive reflectance fusion model for complex heterogeneous regions," *Remote Sensing of Environment*, vol. 114, no. 11, pp. 2610–2623, Nov. 2010.

[46] F. Gao, J. Masek, M. Schwaller, and F. Hall, "On the Blending of the Landsat and MODIS Surface Reflectance : Predicting Daily Landsat Surface Reflectance," *IEEE Transactions on Geoscience and Remote Sensing*, vol. 44, no. 8, pp. 2207–2218, 2006.

**Jiaqi Tian** received his B.M. degree in land resource management from Northeast Agricultural University, Harbin, China, in 2014 and the M.Sc. degree in geomatics from The Hong Kong Polytechnic University, in 2016.

He is currently a Ph.D. student of Department of Land Surveying and Geo-Informatics, The Hong Kong Polytechnic University. His research interests include satellite vegetation phenology.

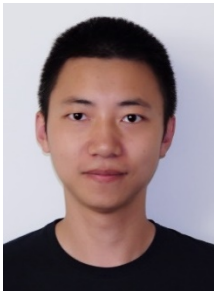

**Xiaolin Zhu** received his B.Sc. degree in resource science and engineering and M.Sc. in civil engineering from Beijing Normal University, in 2007 and 2010, respectively. He received his Ph.D. degree in geography at Ohio State University in 2014. He was postdoctoral researcher at Colorado State University and University of California, Davis in 2015 and 2016, respectively.

He is currently an Assistant Professor at Department of Land Surveying and Geo-Informatics, The Hong Kong Polytechnic University. His research interests include remote sensing, geospatial analysis, and urban and ecological studies.

**Luoma Wan** received the B.Sc. degree in computer science and technology from Wuhan Institute of Technology, Wuhan, China, in 2012, the M.Sc. degree in software engineering from South China Normal University, Guangzhou, China, in 2015, and the Ph.D. degree in earth system and geoinformation science at the Chinese University of Hong Kong, Hong Kong, in 2021. From 2015 to 2018, he was a Research Assistant with the Institute of Space and Earth Information Science, Chinese University of Hong Kong. His research interests include mangrove forests monitoring with remote sensing and deep learning.

**Melissa Collin** received the B.Sc. degree in environmental science and management from Humboldt State University, Arcata, CA, USA, in 2019, where she is currently working toward the M.Sc. degree in environmental science and management, concentrating in geospatial science.

She is currently a Research Assistant with Humboldt State University. Her research interests include remote sensing and geospatial science.